euspen's 26th International Conference & Exhibition, Krakow, PL, June 2026
www.euspen.eu

Telecentric Under-Surface Imaging System for In-situ Observation of Polishing Pad–Glass Contact

Adam Wilczek[1], Nico Zettler[1], Prof. Dr. Rainer Börret[1]

[1]*Aalen University, Center for Optical Technologies (ZOT), Beethovenstr. 1, 73430 Aalen, Germany*

adam.wilczek@hs-aalen.de

Abstract

In computer-controlled optical polishing, direct observation of pad–surface contact is hindered by slurry, refractive interfaces, and motion. We present a telecentric under-surface imaging system that records pad–glass contact through the workpiece during force-controlled polishing of N-BK7 (10 N, ~830 rpm). A 5 MP camera with a telecentric objective acquires images at ~12 fps while a coaxial LED module provides uniform illumination. We report quantitative characterization of the imaging system: spatial resolution of approximately 50 µm (sufficient to resolve individual pad pores), illumination uniformity within ±5 % across the aperture, motion blur of ~180 µm at 350 µs exposure, and frame-to-frame intensity variation below 1.1 %. The pulsed illumination mode enables short exposures despite surface speeds exceeding 0.5 m/s. In-situ imaging reveals the heterogeneous contact distribution created by the porous pad microstructure and captures previously undocumented phenomena including progressive contact intensity changes and slurry sedimentation patterns. Comparison of accumulated contact maps with white-light interferometry measurements confirms qualitative correspondence with material removal profiles.

telecentric imaging, in-situ metrology, illumination uniformity, high-speed vision, optical polishing instrumentation

1. Introduction

Computer-controlled optical polishing relies on precise control of the pad–workpiece interaction to achieve deterministic material removal [1]. According to the Preston equation, removal rate depends on contact pressure and relative velocity [2]. Finite element simulations have been employed to model elastic pad deformation and predict material removal based on calculated pressure distributions [3], and dwell time algorithms optimize tool paths to correct surface figure errors through controlled local removal [4]. However, these models typically assume a time-invariant, spatially uniform tool influence function (TIF) derived from Gaussian or Hertzian contact mechanics.

Recent work has shown that the TIF during sub-aperture polishing is influenced by numerous factors including pad porosity, slurry transport, and spatially varying friction coefficients [5]. Comprehensive reviews of dwell time optimization highlight that TIF stability remains a key challenge for achieving sub-nanometer surface accuracy [6]. While analytical TIF models have been developed for curved surfaces [7] and microscale contact mechanics have been studied for porous pads [8], experimental validation of the actual contact distribution, particularly the heterogeneous contact created by porous pad microstructures, remains limited.

Various in-situ monitoring approaches have been developed for chemical mechanical polishing (CMP). Evanescent-wave microscopy enables nanoscale observation of slurry particle behavior near the contact interface [9], while dual-emission laser-induced fluorescence (DELIF) provides high-resolution maps of slurry film thickness beneath transparent substrates [10]. Interferometric methods have been applied for in-situ pad surface characterization [11], and sensor-based approaches using accelerometers or force transducers monitor process stability [12]. However, these techniques either require specialized optical setups incompatible with rotating tools, operate at microscopic scales unsuitable for full-pad observation, or provide indirect measurements rather than direct contact imaging.

For sub-aperture polishing with small rotating pads, direct imaging of the pad–glass contact presents specific challenges: the imaging system must capture the entire pad area (~12 mm diameter) at sufficient resolution to resolve pore structures (~50–200 µm), maintain sharp images despite surface speeds exceeding 0.5 m/s, and provide uniform illumination without introducing reflections from the slurry-filled interface.

In this work, we present the design and characterization of a telecentric under-surface imaging system for in-situ observation of pad–glass contact during optical polishing. The system employs a telecentric objective with coaxial illumination to image through transparent N-BK7 substrates at approximately

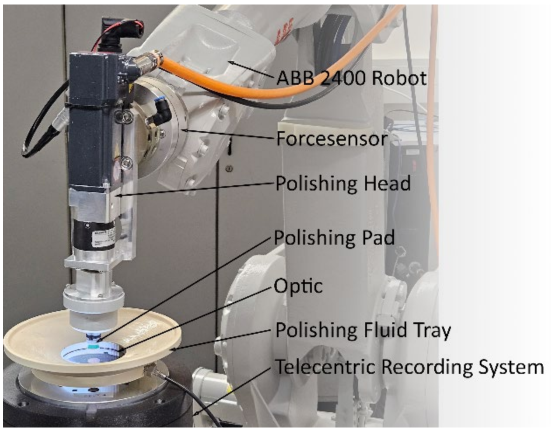

Figure 1. Experimental setup showing all components of the polishing system.

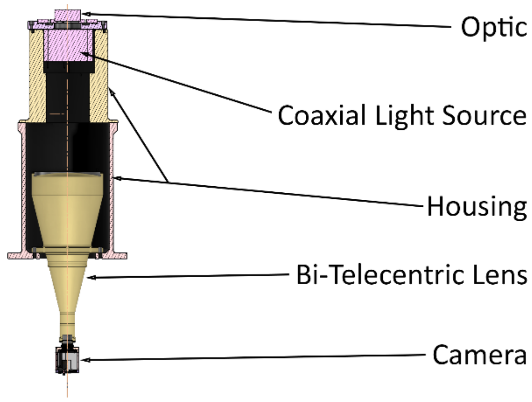

Figure 2. Schematic of the telecentric imaging system with individual components.

12 frames per second. We report quantitative characterization of resolution, illumination uniformity, and motion blur, and demonstrate pore-resolved contact imaging under process conditions. A companion submission to this conference addresses the use of these image sequences for constructing pore-aware dwell maps.

2. Experimental Setup

The experimental setup comprises three main subsystems (figure 1): a robotic positioning system, a rotating polishing head, and a telecentric imaging unit mounted beneath the workpiece.

2.1. Polishing system

An ABB IRB 2400 industrial robot (ABB Ltd., Switzerland) positions the polishing head across the workpiece surface. A force sensor mounted between the robot flange and the polishing head enables force-controlled operation in the vertical direction. The polishing head carries a porous polyurethane pad (12 mm diameter) driven by a pneumatic spindle at approximately 830 rpm. Motor control is implemented using a Beckhoff automation system. Trajectory planning is performed using in-house developed software (Zaphod, Pandora).

All experiments were conducted on plane-parallel N-BK7 glass substrates (65 mm diameter) with surface form deviation below 3 µm. The substrates were mounted in a retaining ring that holds a stationary slurry bath, ensuring the glass surface remains submerged approximately 1–2 mm below the slurry level throughout polishing. Cerium oxide slurry was prepared at a 10:1 ratio of deionized water to abrasive. No slurry circulation was employed.

The polishing trajectory follows a meander pattern with 14 mm path spacing at a constant normal force of 10 N. This spacing exceeds the pad diameter, resulting in non-overlapping passes—a deliberate choice to isolate individual track signatures for validation purposes.

2.2 Telecentric imaging system

The imaging system is positioned beneath the transparent substrate to capture the pad–glass contact zone during polishing (figure 2). The optical path comprises four main components: substrate holder, coaxial illumination module, telecentric objective, and camera.

The N-BK7 substrate is bonded at its periphery using optical wax, leaving a central aperture clear for imaging. Both substrate surfaces were polished to better than 10 nm RMS roughness prior to mounting, ensuring high optical transmission in the visible range (380–780 nm).

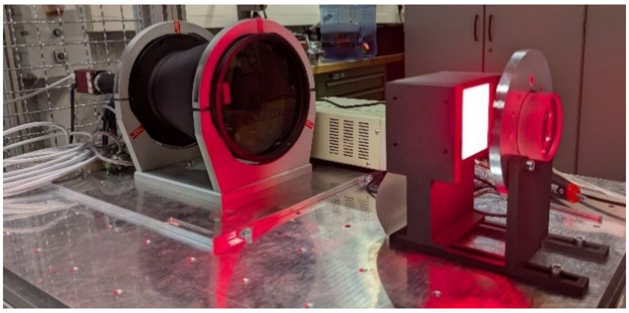

Figure 3. Experimental setup showing camera with telecentric objective (left), coaxial illumination module (red), and test substrate (right).

Illumination is provided by a coaxial LED module (FLFV-Si70N2-IP65-W, Falcon Illumination) with a 70 mm × 70 mm field of view. Coaxial geometry was selected over ring illumination to eliminate specular reflections from the LED array and camera objective that had caused artifacts in earlier setups. The LED module is synchronized with the camera exposure, enabling pulsed operation at approximately three times the continuous power rating. This increased intensity permits exposure times of 350 µs, which is critical for minimizing motion blur at the pad's peripheral velocity (~0.5 m/s).

The imaging optics consist of a telecentric objective (TC23110, Opto Engineering) coupled to a 5-megapixel monochrome camera (Manta G-504B, Allied Vision). The telecentric design maintains constant magnification regardless of object distance within the depth of field, eliminating perspective distortion that would otherwise affect contact area measurements. The complete optical assembly is enclosed in a 3D-printed housing (black PLA) to exclude ambient light. Figure 3 shows the individual components prior to integration.

Table 1 summarizes the key specifications of the imaging system.

Table 1. Specifications of the telecentric imaging system.

Parameter	**Value**
Camera	Allied Vision Manta G-504B
Resolution	5 MP (2452 × 2056 pixels)
Frame rate	~12 fps
Objective	Opto Engineering TC23110
Field of view	70 mm × 70 mm (limited by substrate: 65 mm)
Spatial resolution	~43 µm/pixel
Exposure time	350 µs
Illumination	Coaxial LED, pulsed

3. Image Quality Characterization

To validate the imaging system for quantitative contact analysis, we characterized its optical performance in terms of spatial resolution, illumination uniformity, and motion blur.

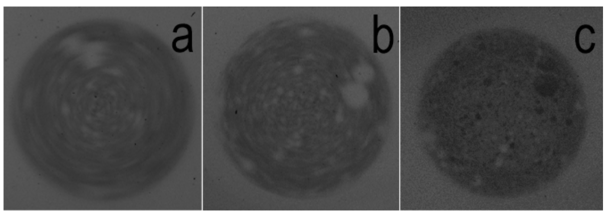

Figure 5. Pad images at different exposure times: (a) 3172 µs, (b) 1500 µs, and (c) 350 µs, demonstrating reduced motion blur with shorter exposure.

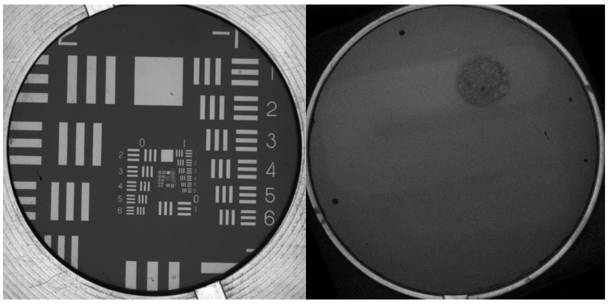

Figure 4. Left: USAF 1951 resolution target imaged through the telecentric optical system with N-BK7 substrate in place. Right: Representative in-situ image during polishing showing the 12 mm diameter pad in the slurry bath at approximately 830 rpm.

3.1 Spatial resolution

Spatial resolution was assessed using a United States Airforce (USAF) 1951 resolution target (figure 4). Under static conditions with the target positioned at the nominal working distance, line pairs in Group 3, Element 3 (approximately 50 µm feature size) were clearly resolved. This resolution is sufficient to distinguish individual pad pores, which typically range from 100 to 500 µm in diameter for the polyurethane pads used in this study.

The telecentric objective provides an extended depth of field exceeding 5 mm, ensuring that the pad–glass contact remains in focus despite minor axial displacement during polishing.

3.2 Illumination uniformity

Illumination uniformity was evaluated from flat-field images acquired through the substrate without the polishing pad present. The coaxial illumination geometry produced highly uniform intensity across the 65 mm aperture, with pixel intensity varying by less than ±5 % from the mean value (excluding the peripheral region outside the substrate).

Compared to earlier setups using ring illumination, the coaxial configuration eliminated three critical artifacts: (i) specular reflections of individual LEDs visible in the image, (ii) intensity gradients caused by non-uniform illumination angles, and (iii) thermal drift due to LED heating during extended acquisition. The enclosed housing further improved stability by excluding ambient light.

3.3 Motion blur

At a spindle speed of 830 rpm, the pad periphery moves at approximately 0.53 m/s. Motion blur was evaluated by imaging edge transitions at various exposure times (figure 5). At exposure times exceeding 500 µs, edges appeared visibly blurred. Reducing the exposure to 350 µs decreased the transition width to approximately 180 µm (corresponding to ~4 pixels), which is acceptable given the target pore sizes.

Further reduction of exposure time improved edge sharpness but increased image noise due to reduced photon count. The pulsed illumination mode, which delivers approximately three times the continuous LED power, was essential to maintain adequate signal-to-noise ratio at 350 µs exposure. This exposure time represents an optimized trade-off between motion blur and image noise for the current hardware configuration.

3.4 Temporal stability

Frame-to-frame intensity stability was assessed by acquiring 1000 consecutive frames under constant illumination without the polishing pad. The mean intensity varied by less than 1.1 % (standard deviation) across the sequence, confirming stable illumination and sensor response over the typical duration of a polishing experiment (~90 s, ~1000 frames).

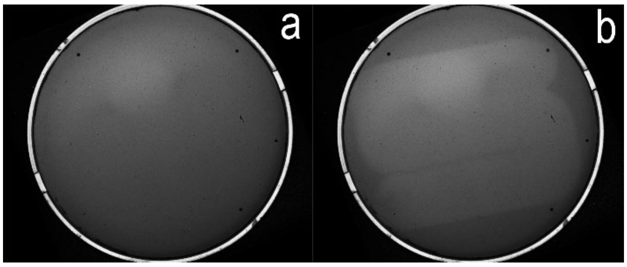

Figure 6. Substrate (a) before and (b) after polishing, showing slurry sedimentation patterns.

Table 2 summarizes the measured imaging performance parameters.

Table 2. Measured imaging performance.

Parameter	Value
Spatial resolution	~50 µm (USAF Gr. 3-3)
Illumination uniformity	±5 % (radial)
Motion blur at 350 µs	~180 µm (~4 pixels)
Frame-to-frame intensity variation	< 1.1 % (std)

4. Results

4.1 In-situ imaging during polishing

All polishing experiments were conducted in a climate-controlled environment at 21 °C ± 1 K. Figure 4 right shows a representative in-situ image acquired during polishing at 10 N normal force and approximately 830 rpm spindle speed.

The porous pad microstructure is clearly visible in the contact zone. Dark regions correspond to pad material in contact with the glass surface, while bright regions indicate pores where no contact occurs. The pad boundary is well-defined, enabling automated detection of the pad position and diameter in each frame.

Three reference holes drilled into the substrate periphery (visible in figure 4 right) serve as fiducial markers for registering the camera images to subsequent white-light interferometry (WLI) measurements. Minor contamination particles on the optical surfaces are visible as stationary spots in the image; these were not removed during the current experiments but affect only a small fraction of the field of view.

4.2 Observed contact phenomena

The in-situ image sequences revealed several phenomena relevant to polishing process understanding:

Slurry sedimentation. In the stationary slurry bath configuration, sedimentation of abrasive particles was observed over time. Figure 6 compares images acquired before and after a polishing run. The polished track appears brighter than the surrounding area, indicating that slurry particles have settled preferentially in regions where no pad contact occurred. The magnitude of this sedimentation effect has not yet been quantified.

Progressive contact intensity change. During each polishing run, the pad contact regions became progressively darker over three to four meander passes. This observation suggests that the imaging contrast evolves as the pad conditions into the slurry, possibly due to slurry absorption into the pad pores, removal of a surface layer from the pad, or smoothing of the glass surface increasing optical contact.

Pad wear signatures. Repeated imaging of the same pad across multiple experiments revealed gradual changes in the pore pattern consistent with pad wear and glazing. While not systematically quantified in this work, these observations

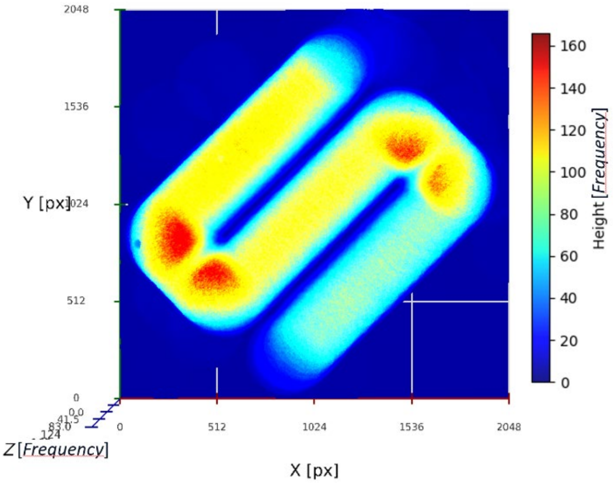

Figure 7. Accumulated contact intensity map from in-situ image sequence.

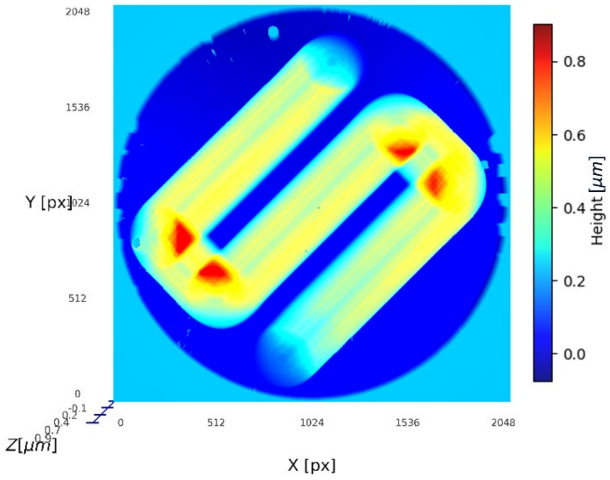

Figure 8. Material removal profile measured by white-light interferometry (Zygo NewView 8300).

demonstrate the system's potential for in-situ pad condition monitoring.

4.3 Comparison with interferometric measurements

To validate that the in-situ contact images correlate with actual material removal, we compared temporally accumulated contact maps with WLI-measured removal profiles. Figure 7 shows a contact accumulation map generated by summing the contact intensity across all frames of a polishing experiment. Figure 8 shows the corresponding material removal measured by WLI (Zygo NewView 8300).

The two maps exhibit clear qualitative correspondence: the meander trajectory pattern is visible in both, and regions of higher accumulated contact generally correspond to regions of greater material removal. However, several systematic differences are apparent:

(i) The accumulated contact map does not capture the characteristic removal depression along the track centerline visible in the WLI data.

(ii) Start and end positions of the polishing path show spatial offsets between camera and WLI data.

(iii) The 90° turns in the meander pattern appear more pronounced in the contact accumulation than in the measured removal.

These discrepancies indicate that raw contact accumulation alone does not fully predict material removal. A companion submission to this conference addresses these limitations through radial velocity correction, drift compensation, and edge weighting.

5. Conclusion and Outlook

We have presented the design and characterization of a telecentric under-surface imaging system for in-situ observation of pad–glass contact during optical polishing. The system achieves a spatial resolution of approximately 50 µm, sufficient to resolve individual pad pores, while operating at ~12 fps with 350 µs exposure to minimize motion blur at typical polishing speeds. Coaxial illumination provides uniform lighting across the 65 mm substrate aperture and eliminates reflection artifacts that affected earlier configurations.

The imaging system successfully captures the heterogeneous contact distribution created by the porous pad microstructure. In-situ observations revealed previously undocumented phenomena including progressive contact intensity changes during polishing and slurry sedimentation patterns in stationary bath configurations. Comparison with interferometric removal measurements confirmed qualitative correspondence between accumulated contact and material removal, while also identifying systematic deviations that require model-based correction.

Future development includes synchronizing the camera trigger with the spindle encoder for phase-locked acquisition, enabling analysis of pad deformation during rotation. Upgrading to a camera with higher frame rate, resolution, and quantum efficiency would improve temporal sampling, resolve smaller pore structures, and permit shorter exposure times with reduced noise.

The current visible-spectrum operation (380–780 nm) is constrained by N-BK7 transmission. Infrared-transmitting substrates (e.g., calcium fluoride) could enable thermal imaging of frictional heating at the pad–glass interface.

Beyond fundamental research, the telecentric imaging approach offers potential for industrial process monitoring, where real-time detection of pad wear, slurry starvation, or contamination could enable closed-loop control.

In summary, the telecentric under-surface imaging system provides a validated platform for pore-resolved observation of pad–glass contact, enabling both fundamental process understanding and quantitative data acquisition for predictive removal models.

Acknowledgement

This research is part of the "MoKI-pro" project (Grant No. 13FH114KA1), funded by Bundesministerium für Bildung und Forschung, and conducted at Aalen University.

References

[1] Li H et al. 2022 Light: Adv. Manuf. 3 28
[2] Preston F W 1927 J. Soc. Glass Technol. 11 214–56
[3] Almeida R et al. 2016 J. Eur. Opt. Soc.-Rapid Publ. 11 16012
[4] Jones R A 1977 Appl. Opt. 16 218–24
[5] Suratwala T et al. 2021 Appl. Opt. 60 201–14
[6] Wang T et al. 2024 Light: Adv. Manuf. 5 21
[7] Wan S et al. 2018 Precis. Eng. 52 332–42
[8] Fu G et al. 2022 Int. J. Mech. Sci. 227 107420
[9] Takahashi Y et al. 2023 Precis. Eng. 82 1–12
[10] Gray C et al. 2004 MRS Proc. 816 K5.8
[11] Park J et al. 2021 Appl. Sci. 11 6839
[12] Schneckenburger M et al. 2022 SN Appl. Sci. 4 21